SCIENTIFIC REPORTS

OPEN

Thermally stable amorphous tantalum yttrium oxide with low IR absorption for magnetophotonic devices

Takuya Yoshimoto[1], Taichi Goto[1,2,3], Hiroyuki Takagi[1], Yuchi Nakamura[1], Hironaga Uchida[1], Caroline A. Ross[3] & Mitsuteru Inoue[1]

Thin film oxide materials often require thermal treatment at high temperature during their preparation, which can limit them from being integrated in a range of microelectronic or optical devices and applications. For instance, it has been a challenge to retain the optical properties of Bragg mirrors in optical systems at temperatures above 700 °C because of changes in the crystalline structure of the high–refractive-index component. In this study, a ~100 nm–thick amorphous film of tantalum oxide and yttrium oxide with an yttrium-to-tantalum atomic fraction of 14% was prepared by magnetron sputtering. The film demonstrated high resistance to annealing above 850 °C without degradation of its optical properties. The electronic and crystalline structures, stoichiometry, optical properties, and integration with magnetooptical materials are discussed. The film was incorporated into Bragg mirrors used with iron garnet microcavities, and it contributed to an order-of-magnitude enhancement of the magnetooptical figure of merit at near-infrared wavelengths.

High temperature processing is essential to the preparation of high-quality functional oxides that exhibit magnetism[1,2], ferroelectricity[3], room-temperature multiferroicity[4,5], and low optical absorption[6]. These properties are used in a range of magnetooptical[7], spintronic[8], magnonic[9,10], ionic[11–13], and multiferroic devices[4]. To integrate materials that require high temperature processing into heterostructures and devices, the thermal stability of other materials in the device is a basic requirement. In particular, integrating functional oxides into optical components—e.g., Bragg mirrors (BMs), one of the best-known optical devices, which are made from alternating layers with high and low refractive indices (n)—is challenging because of the increase in optical losses in the high-n material caused by high temperature annealing.

Tantalum oxide (Ta_2O_5) is widely used as a high-n material in BMs because of its high transmissivity and high heat resistance[14,15]. Compared with other high-n materials, such as titanium oxide (TiO_2)[16] and hafnium oxide (HfO_2)[17,18], Ta_2O_5 has crystallisation and glass-transition temperatures that are approximately 300 °C higher[19]. Despite this, Ta_2O_5 lacks the necessary thermal stability to withstand the annealing required for integration of magnetooptical oxides, such as iron garnets, which may require an 800 °C oxygen annealling in order to fully crystallise and exhibit high Faraday rotation. For example, degradation of the quality of a high-n material decreased the performance of a microcavity, comprising a magnetooptical layer sandwiched between two BMs[19–21].

We previously demonstrated a microcavity in which a cerium-substituted yttrium iron garnet film (CeYIG, $Ce_xY_{3-x}Fe_5O_{12}$, with x ~1.0) was used as the magnetooptical material and Ta_2O_5 and SiO_2 were used in the BMs[19]. The Faraday rotation of the microcavity was 30 times that of the CeYIG film at the localization wavelength; however, the Faraday rotation and transmissivity were lower than the theoretical values calculated by the matrix approach[22]. This degradation was attributed to the crystallisation of the Ta_2O_5 used in the BM during the 800 °C anneal that was performed to crystallise the CeYIG. Hence, to improve the Faraday rotation and transmissivity of the microcavity, the crystallisation of Ta_2O_5 must be suppressed.

[1]Department of Electrical and Electronic Information Engineering, Toyohashi University of Technology, 1-1 Hibari-Ga-Oka, Tempaku, Toyohashi, Aichi, 441-8580, Japan. [2]JST, PRESTO, 4-1-8 Honcho, Kawaguchi, Saitama, 332-0012, Japan. [3]Department of Materials Science and Engineering, Massachusetts Institute of Technology, 77 Massachusetts Avenue, Cambridge, Massachusetts, 02139, USA. Correspondence and requests for materials should be addressed to T.G. (email: goto@ee.tut.ac.jp)
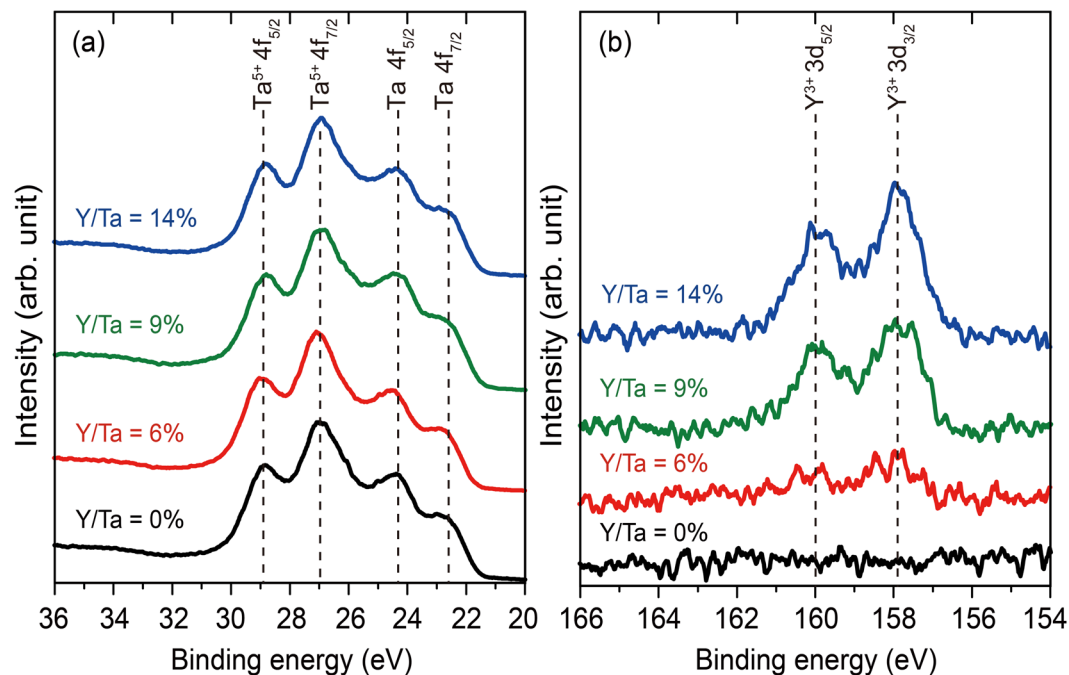
Figure 1. Valence states of the samples. XPS of the as-deposited aTYO and Ta_2O_5 films in the vicinity of the (**a**) Ta^{5+} 4f, Ta 4f and (**b**) Y^{3+} 3d energy levels. The film thickness was 180 nm, and the top 2 nm of each film was etched by Ar^+ to remove the effects of changes in the oxidation state at the surface.

Crystallisation may be suppressed by adding other elements whose ionic radii are larger than those of elements in the base material[23–26]. Toriumi, Yamamoto, *et al*. reported that the crystallisation temperature of HfO_2 was increased by the addition of lanthanum oxide (La_2O_3)[27,28]. The radius of the lanthanum ion is larger than that of the hafnium ion, and La_2O_3 serves to stabilize the amorphous structure in the HfO_2–La_2O_3 film by disrupting the long-range order of crystalline HfO_2. By the same logic, the crystallisation of Ta_2O_5 can also be suppressed by adding another element with a larger ionic radius. Fujikawa and Taga first reported an increase in the crystallisation temperature of Ta_2O_5 caused by addition of yttrium oxide (Y_2O_3)[29]; the effect on current leakage was also reported. However, the optical constants, such as n and the extinction coefficient (κ) of this film—a so-called amorphous tantalum yttrium oxide (aTYO)—were not reported. In other studies, an aTYO was used as a phosphor, and photoluminescence spectra were reported[29–33], but there were no reports on the values of n and κ for the aTYO.

In this work, we prepared an aTYO using magnetron sputtering and investigated its electronic structure, crystallisation temperature, n, and κ. We also used the aTYO to fabricate a microcavity and compared the Faraday rotation and transmissivity of the fabricated microcavity with those of a previously fabricated microcavity using Ta_2O_5. We show that aTYO is a robust amorphous material suitable for integrated optical devices.

Results

Characterisation of Valence States. The X-ray photoelectron spectra (XPS; SXM-CI, ULVAC-PHI, Japan) of the as-deposited aTYO films and a Ta_2O_5 film were measured. Before the XPS measurements, the top 2 nm was etched from each film by Ar^+ milling (bombardment) to remove the effects of surface stoichiometry changes on the oxidation state; the XPS peak positions were then calibrated so that the C 1s peak appeared at the binding energy of 284.8 eV[34]. Figure 1 shows the XPS spectra in the vicinity of the Ta^{5+} 4f, Ta 4f, and Y^{3+} 3d energy levels. In Fig. 1a, the Ta 4f peaks in the spectra of all samples appear at the same position as that for Ta_2O_5, where Y/Ta = 0%. The Ta peak was deconvoluted into four peaks, with contributions coming from the Ta^{5+} at 28.8 eV ($4f_{5/2}$), 26.9 eV ($4f_{7/2}$), and from metallic Ta at 24.3 eV ($4f_{5/2}$) and 22.6 eV ($4f_{7/2}$)[32,35]. The peaks formed a doublet owing to spin-orbit splitting[36]. The metallic states were attributed to reduction induced by Ar^+ bombardment[37]. In Fig. 1b, the two peaks corresponding to Y $3d_{5/2}$ and Y $3d_{3/2}$ appear at the same positions (157.9 eV and 160.0 eV, respectively)[34] regardless of the amount of yttrium in the aTYO. The peak positions of Y^{3+} $3d_{5/2}$ and Y^{3+} $3d_{3/2}$ for aTYO were previously reported to be 157.5 eV and 159.6 eV[32,38], respectively, which are slightly lower energy than the peak positions obtained in this study; however, these results are consistent with the Y^{3+} found in Y_2O_3[34,39] or $YTaO_4$[32]. Changes in the Y/Ta atomic ratio from 6% to 14% did not affect the valence states of Y and Ta in aTYO.

X-ray Characterisation. The X-ray diffraction (XRD; RINT-2500, Rigaku, Japan) patterns of a Ta_2O_5 film and an aTYO films whose atomic fraction was 14% Y were measured to investigate their thermal stability after the addition of Y_2O_3 to Ta_2O_5. The films were annealed in a glass chamber at various temperatures for 30 min in residual air at a pressure of 15 Pa (111 mTorr), which was chosen because this is a suitable condition
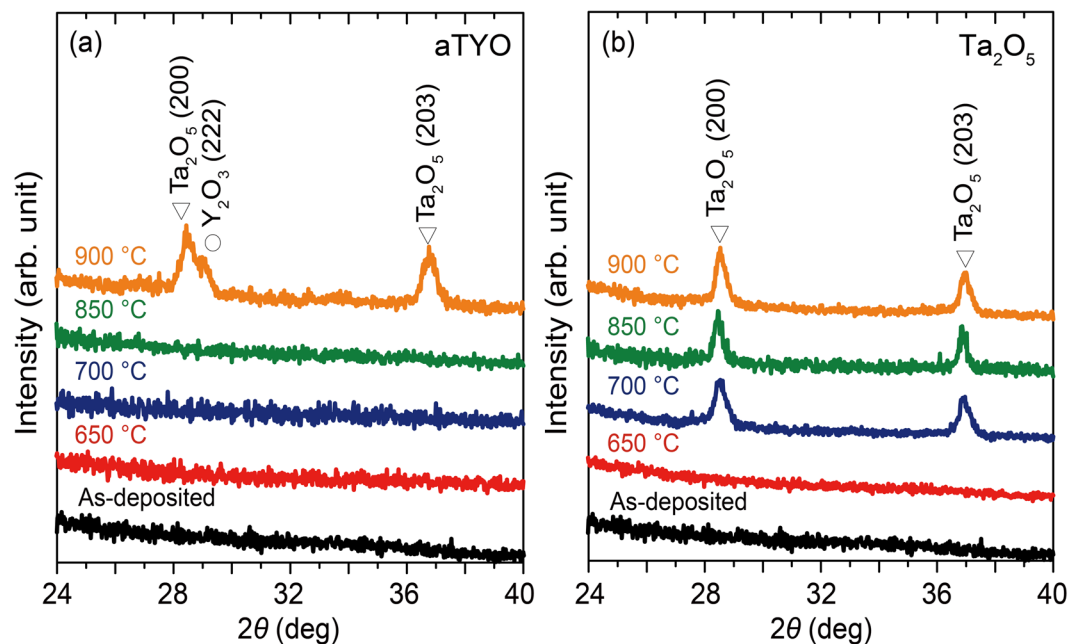
Figure 2. Crystalline states of the samples. XRD patterns of the annealed (**a**) aTYO films at 14% Y and (**b**) Ta_2O_5 films. Annealing was performed for 30 min in residual air at a pressure of 15 Pa (111 mTorr) and temperatures of 650 °C, 700 °C, 850 °C, or 900 °C. The white triangles indicate the diffraction peaks of Ta_2O_5[47], and the white circle indicates the diffraction peak of Y_2O_3[54].

for the crystallisation of CeYIG on the BM[19]. A Cu Kα source at a wavelength of 0.1541 nm was used in the ω–2θ thin-film geometry XRD measurements, and the samples were tilted by 5° to eliminate the substrate peaks. Figure 2 shows the XRD patterns of aTYO and Ta_2O_5. The aTYO annealed at 900 °C exhibits peaks corresponding to those of Ta_2O_5 and Y_2O_3, but aTYO annealed at temperatures below 850 °C was in the amorphous state. The samples are too small to measure melting point and glass transition temperatures using thermogravimetric analysis or other bulk techniques, but they are described here as amorphous because they showed no nanocrystallinity by transmission electron microscopy (see below) and in XRD they exhibited a broad halo at $2\theta \approx 21°$ with a full width at half maximum from 9° to 17°, similar to as-grown Ta_2O_5 films. The observed halo position did not match any crystalline peaks.

The optimum annealing temperature of CeYIG on BM was 800 °C, which is within the range of stability for aTYO. However, Ta_2O_5 crystallised at temperatures above 700 °C. These results indicate that the crystallisation temperature of Ta_2O_5 increased by approximately 200 °C when Y_2O_3 was added to Ta_2O_5 at an atomic fraction of 14%, and the aTYO is sufficiently stable for integration in devices with CeYIG.

Characterisation of Optical Constants. The transmissivity of the as-deposited and annealed aTYO films with 14% Y and the annealed Ta_2O_5 films was measured with a spectrometer (UV-3100PC, Shimadzu, Japan) to analyse the values of n and κ for each sample. The thicknesses of the as-deposited aTYO film, annealed aTYO film, and annealed Ta_2O_5 film were 320 nm, 320 nm, and 1060 nm, respectively. The annealing conditions were 30 min at 15 Pa residual air[40]. The spectra were fitted with SCOUT software ver. 3 (Techno Synergy, Japan), which calculated the optical interference based on the Fresnel equations.

Figure 3 shows plots of transmissivity, n, and κ as functions of wavelength. The addition of Y_2O_3 to Ta_2O_5 decreased n. At a wavelength of 1470 nm, the refractive indices of Y_2O_3, n_{Y2O3}, annealed Ta_2O_5, n_{Ta2O5}, and annealed aTYO, n_{aTYO}, were 1.90[41], 2.04, and 2.02, respectively. The n_{aTYO} value is close to the $n = 2.02$ calculated from the volume ratio of Y and Ta [$= 0.14 \times n_{Y2O3} + 0.86 \times n_{Ta2O5}$]. After annealing, the n of aTYO decreased. This might be because of expansion of the continuous random network[40,42] of aTYO, as seen in other amorphous materials where the refractive index becomes smaller than the initial state after cooling down (quenching)[43–45].

The κ value of annealed aTYO was also lower than that of annealed Ta_2O_5. At a wavelength of 1470 nm, the extinction coefficients of Y_2O_3, κ_{Y2O3}, annealed Ta_2O_5, κ_{Ta2O5}, and annealed aTYO, κ_{aTYO}, were 7.22×10^{-6}[41], 1.89×10^{-3}, and 1.10×10^{-3}, respectively. The suppression of crystallisation reduced grain boundary contributions to loss, reducing the κ value[46]. The shift of the absorption edge of transmission is related to the electronic structure, specifically, the d orbitals of the transition metals[43]. The change of the Y^{3+} $3d_{5/2}$ state of aTYO, shown in Fig. 1b, might increase the band gap of the amorphous oxide.

These results indicate that the aTYO film is more stable against crystallisation than Ta_2O_5 while maintaining a high n and low κ. Although Y_2O_3 has a much lower κ, its low n means that a Bragg mirror made with Y_2O_3 would require more layers than one made with aTYO.
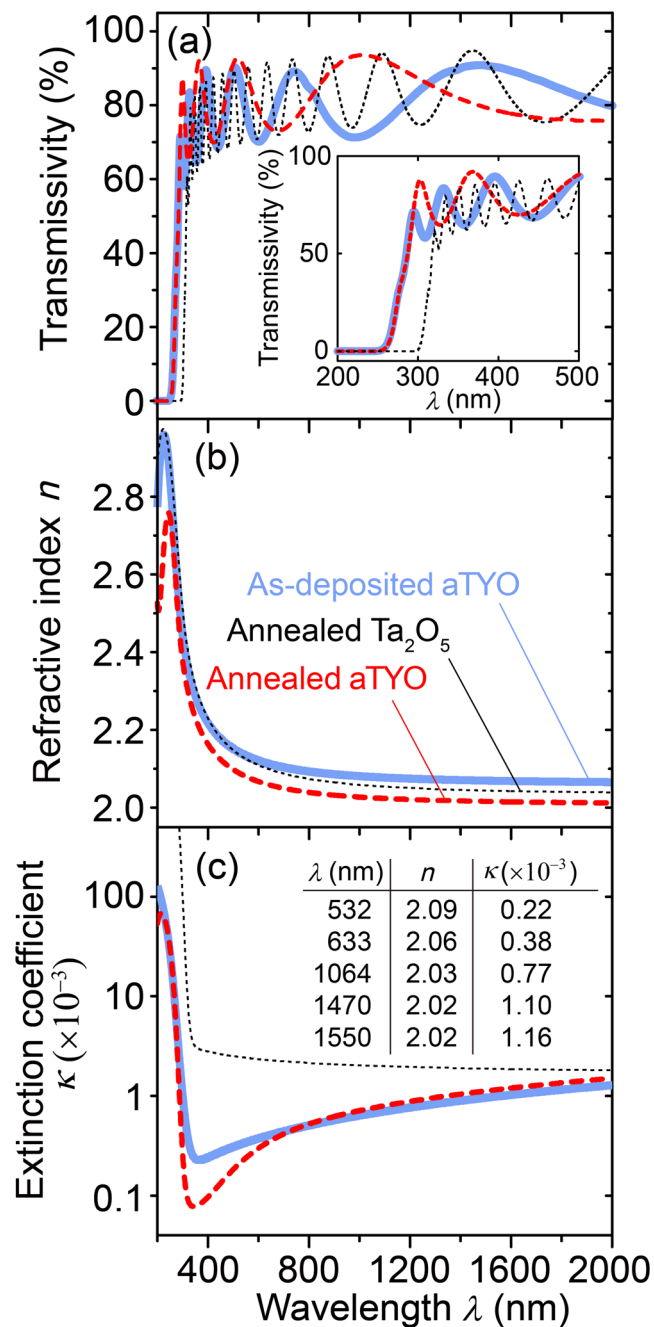
Figure 3. Optical properties of the samples. Plots of the (**a**) transmissivity, (**b**) refractive index (n), and (**c**) extinction coefficient (κ) as functions of the wavelength (λ), obtained by fitting the transmission spectra of each sample. Inset figure in (**a**) shows the enlarged short wavelength region. Inset table in (**c**) shows the n and κ of aTYO at representative wavelengths. Annealing was performed at 800 °C for 30 min in residual air at a pressure of 15 Pa.

Microcavity Structural Analysis. Figure 4a shows a cross-sectional compositional image of the fabricated microcavity obtained with a field-emission scanning electron microscope (FE-SEM; JSM-6700F, JEOL, Japan) using back-scattered electrons, showing a clear layered structure. Not shown in this image, the film exhibited cracks with macroscale (10–100 μm) spacing. Figure 4b shows the profile of propagating light at a wavelength of 1470 nm, calculated as the squared intensity of the electric field in the microcavity using the matrix approach[20]. In this calculation, the actual thicknesses measured from Fig. 4a were used. The incident light was localized at the CeYIG defect layer, which breaks the periodicity of the BM. An enhancement of nonreciprocal effects was expected from this result because the localization increased the interaction between the light and the defect layer.

A transmission electron microscope (TEM; JEM-2100F, JEOL, Japan) was used to obtain images of the fabricated microcavity, in which aTYO or Ta_2O_5 was used in the BM. For the microcavity with aTYO-based BMs, Fig. 4c,d, and e show TEM images of the aTYO film used in the top BM, the CeYIG sandwiched between the two
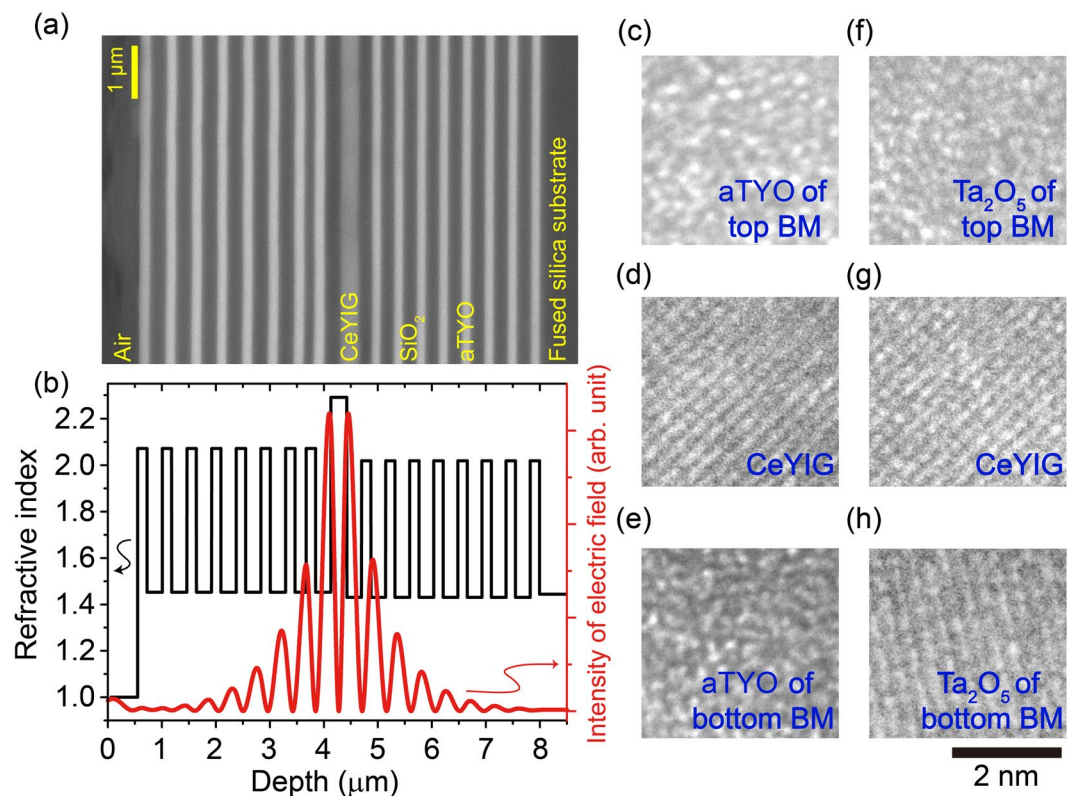
Figure 4. Microcavity structure. (**a**) Cross-sectional compositional image of a fabricated microcavity consisting of silica substrate/[(aTYO/SiO$_2$)^8]/CeYIG/[(SiO$_2$/aTYO)^8]. (**b**) Refractive index profile through the microcavity and intensity of the electric field calculated by the matrix approach. TEM images of (**c**) aTYO used in the top BM, (**d**) CeYIG used in the microcavity composed of aTYO, and (**e**) aTYO used in the bottom BM. TEM images of (**f**) Ta$_2$O$_5$ used in the top BM, (**g**) CeYIG used in the microcavity composed of Ta$_2$O$_5$, and (**h**) Ta$_2$O$_5$ used in the bottom BM.

BMs using aTYO, and the aTYO film used in the bottom BM, respectively. For the microcavity with Ta$_2$O$_5$-based BMs, Fig. 4f,g, and h show TEM images of the Ta$_2$O$_5$ film used in the top BM, the CeYIG sandwiched between the two BMs using Ta$_2$O$_5$, and the Ta$_2$O$_5$ film used in the bottom BM, respectively. Figure 4d and g show the lattice fringes in the magnetic layer of each microcavity, indicating that the CeYIG was crystallised by annealing; the lattice spacings obtained from these images were 0.274 nm with a standard deviation (σ) of 0.008 nm and 0.281 nm with $\sigma = 0.005$ nm, respectively. Both numbers are close to the lattice spacing of 0.277 nm for the (420) plane of garnet, as calculated from the inorganic crystal structure database (ICSD) POWD-12++. The (420) diffraction peak shows the highest intensity of polycrystalline garnets. In contrast, no lattice fringes can be seen in Fig. 4c and f, indicating that the as-deposited aTYO and Ta$_2$O$_5$ were in the amorphous state.

An obvious difference between the two microcavities was observed in the bottom BM. As shown in Fig. 4e, the aTYO layers were amorphous. However, Fig. 4h shows fringes, indicating that the Ta$_2$O$_5$ layers were crystallised. The lattice spacing of Ta$_2$O$_5$ was 0.313 nm ($\sigma = 0.003$ nm), corresponding to the (200) plane of Ta$_2$O$_5$[47], which has the highest peak intensity for obtained polycrystalline Ta$_2$O$_5$. Crystallisation is believed to cause scattering of light, degrading the transmissivity and lowering the Q-factor of the microcavity as discussed below.

We also carried out elemental mapping of the aTYO film by scanning transmission electron microscope and EDX (STEM–EDX) to investigate the distribution of elements. Figure 5a shows a STEM image of an aTYO film used in the top BM, and Fig. 5b,c, and d show EDX mappings of Ta, O, and Y, respectively. These figures indicate that Ta and O were uniformly distributed in the aTYO film, and Y was present in the aTYO. Figure 5a shows varying contrast, but this might be due to the roughness of the prepared sample. No evidence of nanocrystalline regions[48], e.g., inhomogeneous distributions of specific elements, was observed, which is consistent with the XRD results.

Magnetooptical Properties. Figure 6a shows the measured and calculated transmission spectra of the fabricated microcavities. The transmissivity was measured with a spectrometer and the Faraday rotation was measured with a rotating analyser (BH-M600VIR-FKR-TU, Neoark, Japan) by applying a magnetic field of 2 kOe (=160 kA/m) perpendicularly to the films[49]. The incident light at the surface of the sample had a spot size of approximately 2 mm. The halogen lamp was monochromated to give a spectral resolution of approximately 3 nm (the measured wavelength step was 1 nm). The localized mode was observed experimentally at a wavelength of 1470 nm, showing good agreement with the theoretical spectra calculated by the matrix approach[20]. At this wavelength, the propagating light has the profile shown in Fig. 4b; thus, localization in the iron garnet layer was
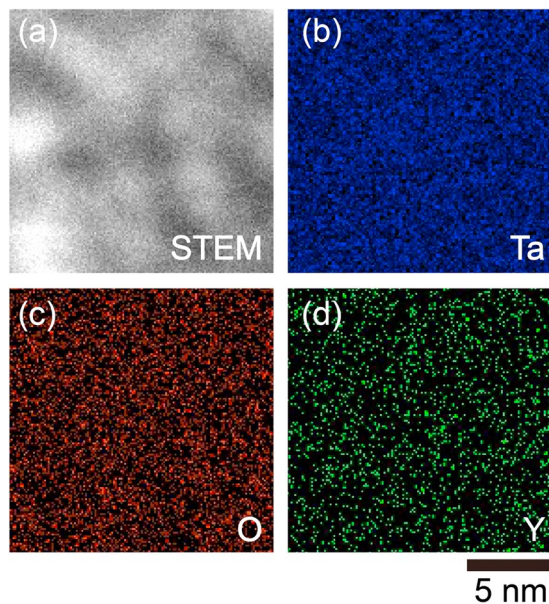
Figure 5. Compositional analysis. (**a**) STEM image of aTYO film used in the top BM. EDX mapping of (**b**) Ta, (**c**) O, and (**d**) Y.

confirmed. In these calculations, we used the actual thicknesses of each layer as determined by the cross-sectional SEM image shown in Fig. 4a and the optical parameters shown in Fig. 3. Other optical parameters of CeYIG, including n and κ, were taken from our previous report[19].

Figure 6b shows an enhanced Faraday rotation of $-5.4°$ and transmissivity of 31% at 1470 nm for the microcavity with aTYO-based BMs. Figure 6c and d show the response in more detail. Compared to the microcavity using Ta_2O_5 in the bottom BM, Faraday rotation was 1.8 times larger ($-2.92°$) and transmissivity was 10 times higher (3%) at the resonant wavelength of each microcavity[20]. However, the Faraday rotation and transmissivity of the aTYO-based microcavity were still low when compared to the calculation results. This is attributed to the variability of the thickness, n, and κ in the layers, to interface roughness, and/or to degradation in transmissivity caused by scattering from the cracks due to thermal mismatch. The broadening of the experimental peaks is attributed to a spatial low coherence within the light beam. Cracks and delamination of the CeYIG and upper layers were introduced after the annealing process. The estimated thermal mismatch strain at 800 °C for the CeYIG, Ta_2O_5, and SiO_2 films were 0.8%, 0.5%, and 0%, respectively, as calculated using the thermal expansion constants of YIG (1.0×10^{-5} K^{-1})[50], Ta_2O_5 (6.7×10^{-6} K^{-1})[51], SiO_2 (5.1×10^{-7} K^{-1})[52], and the fused silica substrate (same as that of SiO_2). Thermal mismatch strain can be reduced by using other substrate materials that have thermal expansion coefficients closer to that of CeYIG or by patterning the substrate so that the cracks form at specific places away from the device area. Nevertheless, these results show the potential of aTYO as a high-n material for the fabrication of optical devices using BMs with high thermal structural stability.

Discussion

The electronic structure, crystallisation temperature, refractive index, and extinction coefficient of aTYO films fabricated by magnetron sputtering were analysed. When the Y/Ta atomic ratio of aTYO was 14%, the crystallisation temperature of aTYO was approximately 200 °C higher than that of Ta_2O_5. The extinction coefficient of aTYO annealed at 800 °C was lower than that of annealed Ta_2O_5 because the aTYO remained amorphous. A microcavity comprising CeYIG and aTYO-based BMs was fabricated as a demonstrative application of aTYO. The Faraday rotation and transmissivity were $-5.4°$ and 31%, respectively, at a wavelength of 1470 nm. These values were respectively 1.8 and 10 times larger than those of a microcavity using crystallised Ta_2O_5 in the bottom BM. These results demonstrate the applicability of aTYO as a high-n material with high thermal stability against crystallisation; they also show the feasibility of using aTYO in BMs to fabricate optical devices resistant to annealing.

Methods

Preparation of aTYO Samples.   Films of aTYO were fabricated on synthetic fused silica (hereafter, silica) substrates by radio-frequency (RF) magnetron sputtering (HSR-551S, Shimadzu, Japan) with various atomic ratios of yttrium/tantalum (Y/Ta). The sputtering target consisted of a Ta_2O_5 disk with a diameter of 10 cm (4 in), on which Y_2O_3 pellets were placed, and the number of Y_2O_3 pellets was changed to vary the Y/Ta atomic ratio. During deposition, Ar gas and O_2 gas were introduced into the chamber at 8.0 cm³ min^{-1} and 2.0 cm³ min^{-1}, respectively. The temperature of the substrate was kept constant at 250 °C, and an RF power of 75 W was applied to the target. The fabricated aTYO film had a thickness of 180 nm. The atomic fractions of the aTYO films were
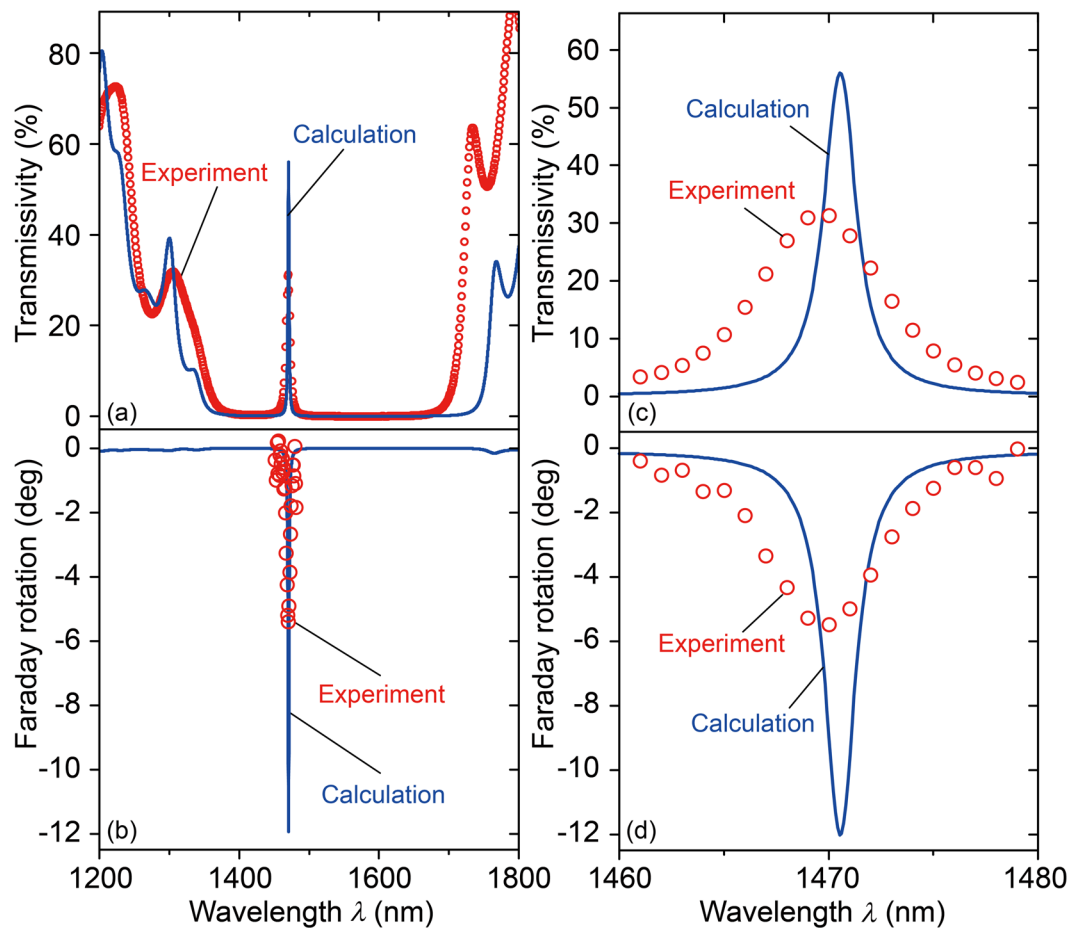
Figure 6. Optical and magnetooptical properties of the microcavity. (**a**) Transmission and (**b**) Faraday rotation spectra of the fabricated microcavity. (**c,d**) Enlarged figures of (**a**) and (**b**) in the vicinity of the peaks. The error bars are smaller than the symbol size.

measured by energy-dispersive X-ray (EDX; JSM-6700F, JEOL, Japan) spectroscopy to be 0% (pure Ta_2O_5), 6%, 9%, and 14% Y.

Preparation of the Microcavity Using aTYO Films in BMs. Sputtered aTYO films were used to fabricate a microcavity with the configuration of silica substrate/[(aTYO/SiO_2)^8]/CeYIG/[(SiO_2/aTYO)^8]. First, the bottom BM, comprising eight layers of aTYO/SiO_2 (represented by [silica substrate/(aTYO/SiO_2)^8]), was prepared by ion-beam sputtering (IBS; OSI-WAVE-IBS, RMtec, Japan) because its deposition rate was higher than that offered by magnetron sputtering. The targets were an aTYO disk whose Y/Ta atomic ratio was 14% and a SiO_2 disk, both of which had diameters of 10 cm (4 in). During the deposition, an RF power of 110 W was applied to the target, the substrate was held at 200 °C, and 7.5 cm^3 min^{-1} of Ar gas and 6.0 cm^3 min^{-1} of O_2 gas were introduced into the chamber. The as-deposited aTYO and SiO_2 had thicknesses of 265 nm and 165 nm, respectively. The center wavelength of the photonic band gap of the bottom BM was 1423 nm according to measurement with a spectrometer.

After the fabrication of the first BM, a 309 nm–thick polycrystalline CeYIG layer was prepared by magnetron sputtering. The film was deposited by applying an RF power of 75 W to a target with a diameter of 10 cm (4 in) in 1.3 Pa (10 mTorr) of Ar gas. The nominal composition of the target was $Ce_{1.0}Y_{2.5}Fe_{5.0}O_{12-\delta}$ (δ shows oxygen deficiency). The substrate was held at 25 °C by water cooling during deposition. The as-deposited CeYIG film was amorphous, and the sample was annealed at 800 °C for 30 min in 15 Pa (111 mTorr) of residual air. After annealing, the top BM, comprising eight layers of aTYO/SiO_2, was fabricated on the CeYIG by IBS using the deposition conditions of the bottom BM without further annealing. The aTYO and SiO_2 used in the top BM had thicknesses of 276 nm and 188 nm, respectively. (The second SiO_2 layer in the top BM was thinner, ~210 nm, because of a mistake during film preparation). The center wavelength of the photonic band gap of the top BM was 1574 nm. The differences in thicknesses and center wavelengths of the photonic band gap between the top and bottom BMs were attributed to several experimental factors. The deposition system was operated manually, leading to unintended variations in layer thickness; furthermore, the bottom BM was annealed, whereas the top BM was not. These issues could be ameliorated by using an *in-situ* thickness monitoring system[21], or bonding of half of the microcavity[53] to ensure identical top and bottom BMs.

References

1. Quindeau, A. *et al*. Tm₃Fe₅O₁₂/Pt heterostructures with perpendicular magnetic anisotropy for spintronic applications. *Adv. Electron. Mater.* **3**, 1600376 (2017).
2. Li, S. *et al*. Epitaxial patterning of nanometer-thick Y₃Fe₅O₁₂ films with low magnetic damping. *Nanoscale* **8**, 388–394 (2016).
3. Rørvik, P. M., Grande, T. & Einarsrud, M.-A. One-dimensional nanostructures of ferroelectric perovskites. *Adv. Mater.* **23**, 4007–4034 (2011).
4. Aimon, N. M., Choi, H. K., Sun, X. Y., Kim, D. H. & Ross, C. A. Templated self-assembly of functional oxide nanocomposites. *Adv. Mater.* **26**, 3063–3067 (2014).
5. Han, H., Kim, Y., Alexe, M., Hesse, D. & Lee, W. Nanostructured ferroelectrics: Fabrication and structure–property relations. *Adv. Mater.* **23**, 4599–4613 (2011).
6. Goto, T., Onbasli, M. C. & Ross, C. A. Magneto-optical properties of cerium substituted yttrium iron garnet films with reduced thermal budget for monolithic photonic integrated circuits. *Opt. Express* **20**, 28507–28517 (2012).
7. Bi, L. *et al*. On-chip optical isolation in monolithically integrated non-reciprocal optical resonators. *Nat. Photon.* **5**, 758–762 (2011).
8. Uchida, K. *et al*. Spin Seebeck insulator. *Nat. Mater.* **9**, 894–897 (2010).
9. Kruglyak, V. V., Demokritov, S. O. & Grundler, D. Magnonics. *J. Phys. D: Appl. Phys.* **43**, 264001 (2010).
10. Serga, A. A., Chumak, A. V. & Hillebrands, B. YIG magnonics. *J. Phys. D: Appl. Phys.* **43**, 264002 (2010).
11. Vohs, J. M. & Gorte, R. J. High-performance SOFC cathodes prepared by infiltration. *Adv. Mater.* **21**, 943–956 (2009).
12. Jung, Y. S., Jung, W., Tuller, H. L. & Ross, C. A. Nanowire conductive polymer gas sensor patterned using self-assembled block copolymer lithography. *Nano Lett.* **8**, 3776–3780 (2008).
13. Phuc, N. H. H., Totani, M., Morikawa, K., Muto, H. & Matsuda, A. Preparation of Li₃PS₄ solid electrolyte using ethyl acetate as synthetic medium. *Solid State Ion.* **288**, 240–243 (2016).
14. Kim, H. & Kim, M. J. Design and characterization of dual-band-pass filters for optical communications. *J. Korean Phys. Soc.* **53**, 1607–1611 (2008).
15. Dods, S. R. A., Zhang, Z. & Ogura, M. Highly dispersive mirror in Ta₂O₅/SiO₂ for femtosecond lasers designed by inverse spectral theory. *Appl. Opt.* **38**, 4711–4719 (1999).
16. Mathews, N. R., Morales, E. R., Cortés-Jacome, M. A. & Toledo Antonio, J. A. TiO₂ thin films – Influence of annealing temperature on structural, optical and photocatalytic properties. *Sol. Energy* **83**, 1499–1508 (2009).
17. Friz, M. & Waibel, F. in *Optical Interference Coatings* (eds Norbert Kaiser & Hans K. Pulker) 105–130 (Springer Berlin Heidelberg, 2003).
18. Durrani, S. M. A. CO-sensing properties of hafnium oxide thin films prepared by electron beam evaporation. *Sensors Actuators B: Chem.* **120**, 700–705 (2007).
19. Yoshimoto, T. *et al*. Magnetophotonic crystal with cerium substituted yttrium iron garnet and enhanced Faraday rotation angle. *Opt. Express* **24**, 8746–8753 (2016).
20. Inoue, M. *et al*. Magnetophotonic crystals. *J. Phys. D: Appl. Phys.* **39**, R151–R161 (2006).
21. Goto, T., Baryshev, A. V., Tobinaga, K. & Inoue, M. Faraday rotation of a magnetophotonic crystal with the dual-cavity structure. *J. Appl. Phys.* **107**, 09A946 (2010).
22. Inoue, M., Levy, M. & Baryshev, A. V. *Magnetophotonics from theory to applications*. (Springer Berlin Heidelberg, 2014).
23. Huang, A. P., Yang, Z. C. & Chu, P. K. in *Advances in Solid State Circuit* Technologies (ed P. K. Chu) 333–350 (InTech, 2010).
24. Zhang, M. H. *et al*. Improved electrical and material characteristics of HfTaO gate dielectrics with high crystallization temperature. *Appl. Phys. Lett.* **87**, 232901 (2005).
25. Ushakov, S. V., Brown, C. E. & Navrotsky, A. Effect of La and Y on crystallization temperatures of hafnia and zirconia. *J. Mater. Res.* **19**, 693–696 (2011).
26. He, W., Zhang, L., Chan, D. S. H. & Cho, B. J. Cubic-structured HfO₂ with optimized doping of lanthanum for higher dielectric constant. *IEEE Electron Device Lett.* **30**, 623–625 (2009).
27. Toriumi, A., Kita, K., Tomida, K. & Yamamoto, Y. Doped HfO₂ for higher-k dielectrics. *ECS Trans.* **1**, 185–197 (2006).
28. Yamamoto, Y., Kita, K., Kyuno, K. & Toriumi, A. Structural and electrical properties of HfLaOₓ films for an amorphous high-k gate insulator. *Appl. Phys. Lett.* **89**, 032903 (2006).
29. Fujikawa, H. & Taga, Y. Effects of additive elements on electrical properties of tantalum oxide films. *J. Appl. Phys.* **75**, 2538–2544 (1994).
30. Blasse, G. & Bril, A. Luminescence phenomena in compounds with fergusonite structure. *J. Lumin.* **3**, 109–131 (1970).
31. Karsu, E. C. *et al*. Luminescence study of some yttrium tantalate-based phosphors. *J. Lumin.* **131**, 1052–1057 (2011).
32. Noto, L. L., Pitale, S. S., Ntwaeaborwa, O. M., Terblans, J. J. & Swart, H. C. Cathodoluminescent stability of rare earth tantalate phosphors. *J. Lumin.* **140**, 14–20 (2013).
33. Kazakova, L. I., Dubovsky, A. B., Semenkovich, G. V. & Ivanova, O. A. Luminescence of YTaO₄ single crystals. *Radiat. Measur.* **24**, 359–360 (1995).
34. Barreca, D., Battiston, G. A., Berto, D., Gerbasi, R. & Tondello, E. Y₂O₃ thin films characterized by XPS. *Surf. Sci. Spectra* **8**, 234–239 (2001).
35. Thomas, J. H. & Hammer, L. H. A photoelectron spectroscopy study of CF₄/H₂ reactive ion etching residue on tantalum disilicide. *J. Electrochem. Soc.* **136**, 2004–2010 (1989).
36. Prieto, P., Galán, L. & Sanz, J. M. Changes induced in the secondary electron emission properties of tantalum nitride by Ar⁺ bombardment and oxygen exposure. *Appl. Surf. Sci.* **70**, 186–190 (1993).
37. Ho, S. F., Contarini, S. & Rabalais, J. W. Ion-beam-induced chemical changes in the oxyanions (Moyn-) and oxides (Mox) where M = chromium, molybdenum, tungsten, vanadium, niobium and tantalum. *J. Phys. Chem.* **91**, 4779–4788 (1987).
38. Choi, S. C. *et al*. Heteroepitaxial growth of Y₂O₃ films on Si(100) by reactive ionized cluster beam deposition. *Nucl. Instr. Meth. Phys. Res. B* **121**, 170–174 (1997).
39. Gauzzi, A., Mathieu, H. J., James, J. H. & Kellett, B. AES, XPS and SIMS characterization of YBa₂Cu₃O₇ superconducting high Tc thin films. *Vacuum* **41**, 870–874 (1990).
40. Bates, S. *et al*. Analysis of amorphous and nanocrystalline solids from their x-ray diffraction patterns. *Pharm. Res.* **23**, 2333–2349 (2006).
41. Nigara, Y. Measurement of the optical constants of yttrium oxide. *Jpn. J. Appl. Phys.* **7**, 404 (1968).
42. Sestak, J., Mares, J. J. & Hubik, P. *Glassy, Amorphous and Nano-Crystalline Materials*. (Springer Berlin Heidelberg, 2010).
43. De Jong, B. H. W. S., Beerkens, R. G. C., van Nijnatten, P. A. & Le Bourhis, E. in *Ullmann's Encyclopedia of Industrial Chemistry*, 1–54 (Wiley-VCH Verlag GmbH & Co. KGaA, 2000).
44. Lillie, H. R. & Ritland, H. N. Fine annealing of optical glass. *J. Am. Ceram. Soc.* **37**, 466–473 (1954).
45. Winter, A. Transformation region of glass. *J. Am. Ceram. Soc.* **26**, 189–200 (1943).
46. Suzuki, Y. *et al*. Selective crystallization of magnetic garnet films on Bragg mirrors by laser annealing. *J. Magn. Soc. Jpn.* **36**, 183–187 (2012).
47. Moser, R. Single-crystal growth and polymorphy of Nb₂O₅ and Ta₂O₅. *Schweiz. Mineral. Petrogr. Mitt.* **45**, 35–101 (1965).
48. Murray, C. B., Norris, D. J. & Bawendi, M. G. Synthesis and characterization of nearly monodisperse CdE (E = sulfur, selenium, tellurium) semiconductor nanocrystallites. *J. Am. Chem. Soc.* **115**, 8706–8715 (1993).

49. Goto, T. *et al*. Vacuum annealed cerium-substituted yttrium iron garnet films on non-garnet substrates for integrated optical circuits. *J. Appl. Phys.* **113**, 17A939 (2013).
50. Geller, S., Espinosa, G. P. & Crandall, P. B. Thermal expansion of yttrium and gadolinium iron, gallium and aluminum garnets. *J. Appl. Crystallogr.* **2**, 86–88 (1969).
51. Wu, S., Chan, H. M. & Harmer, M. P. Compositional tailoring of the thermal expansion coefficient of tantalum (V) oxide. *J. Mater. Sci.* **41**, 689–695 (2006).
52. Kühn, B. & Schadrack, R. Thermal expansion of synthetic fused silica as a function of OH content and fictive temperature. *J. Non-Cryst. Solids* **355**, 323–326 (2009).
53. Haga, Y., Goto, T., Baryshev, A. V. & Inoue, M. One-dimensional single- and dual-cavity magnetophotonic crystal fabricated by bonding. *J. Magn. Soc. Jpn.* **36**, 54–57 (2012).
54. Baldinozzi, G., Berar, J. F. & Calvarin, G. Rietveld refinement of two-phase Zr-doped Y_2O_3. *Mater. Sci. Forum* **278–281**, 680–685 (1998).

Acknowledgements

Author Contributions

T.Y., and T.G. prepared and characterised the samples. T.Y. calculated the transmission and Faraday rotation spectra. C.R. analysed the numerical data. H.T., Y.N., and M.I. supervised the experimental setups. T.G. wrote the manuscript with inputs from H.U. and C.R.

Additional Information